Journal of Molecular Structure 1164 (2018) 9–22

Contents lists available at ScienceDirect

Journal of Molecular Structure

journal homepage: http://www.elsevier.com/locate/molstruc

Insights into the structural/conformational requirements of cytotoxic oxadiazoles as potential chemotherapeutic target binding agents

Radin Alikhani [a], Nima Razzaghi-Asl [a, *], Ali Ramazani [b], Zahra Hosseinzadeh [b]

[a] Department of Medicinal Chemistry, School of Pharmacy, Ardabil University of Medical Sciences, PO Box: 5618953141, Ardabil, Iran
[b] Department of Chemistry, University of Zanjan, P.O. Box 45195-313, Zanjan, Iran

ARTICLE INFO

Article history:
Available online 13 March 2018

Keywords:
Cytotoxicity
Oxadiazole
Docking
Quantum mechanical

ABSTRACT

A few novel previously synthesized 2,5-disubstituted 1,3,4-oxadiazoles with cytotoxic activity (**1**–**17**) were subjected to combined docking/quantum mechanical studies against chemotherapeutic targets. Selected macromolecular targets were those that were previously known to be inhibited by 1,3,4-oxadiazoles. Within this work, favorable binding modes/affinities of the oxadiazoles toward validated cancer targets were elucidated. Some oxadiazole structures exhibited ΔG_bs comparable to or stronger than crystallographic ligands that were previously demonstrated to inhibit such targets. On the basis of obtained results, a general structure activity/binding relationship (SAR/SBR) was developed and a few 2,5-disubstituted 1,3,4-oxadiazole structures were proposed and virtually validated as potential cytotoxic candidates. To get more insight into structure binding relationship of candidate molecules within best correlated targets, docked conformation of the best *in silico in vitro* correlated oxadiazole structure was analyzed in terms of intermolecular binding energy components by functional B3LYP in association with split valence basis set using polarization functions (Def2-SVP). We believe that such modeling studies may be complementary to our previous results on the synthesis and cytotoxicity assessment of novel 1,3,4-oxadiazole derivatives through extending the scope of privileged structures toward designing new potential anti-tumor compounds.

1. Introduction

Compounds possessing diverse heterocyclic nucleuses have obtained special significance in drug discovery and design. Among such privileged scaffolds, five-membered 1,3,4-oxadiazole ring has attracted considerable concern in medicinal chemistry due to the broad range of pharmaceutical and biological activities, such as anticancer [1], antifungal [2], antibacterial [3], antiviral [4], analgesic [5], anti-inflammatory [6], antihypertensive [7], anti-convulsant [8] and anti-diabetic [9] effects. Moreover, various synthetic approaches toward 1,3,4-oxadiazoles have facilitated the investigation of their chemical and biological properties.

A number of 2,5-disubstituted 1,3,4-oxadiazole structures have been reported to exhibit cytotoxic activity through the inhibition of different growth factors, enzymes and kinases including telomerase, histone deacetylase (HDAC), methionine aminopeptidase (MetAP), thymidylate synthase (TS), glycogen synthase kinase-3 (GSK), epidermal growth factor (EGF), vascular endothelial growth factor (VEGF) and focal adhesion kinase (FAK) [10].

Among mentioned targets, the major mechanism responsible for anticancer potency of 1,3,4-oxadiazole derivatives relates to the inhibition of telomerase enzyme. In a few separated studies, different 1,3,4-oxadiazole derivatives were synthesized and screened for their telomerase inhibitory activity against MCF-7 and other cancer cell lines. The major assessed compounds were 1,4-benzodioxane, 2-chloro pyridine, acyl hydrazone and quinoline containing 1,3,4-oxadiazole derivatives [11–14].

Structure activity relationship (SAR) studies of two different series of synthetic 1,3,4-oxadiazoles revealed that for HDAC inhibition three pharmacophoric requirements are zinc binding group, linker and surface recognition cap group [15]. HDAC inhibitors can suppress the phosphorylation of human telomerase reverse transcriptase (hTRT) by protein kinase B (PKB/Akt) through regulation of telomerase activity [16]. This can represent an innovative strategy to design compounds which co-targets (PKB-Akt) and

* Corresponding author. Department of Medicinal Chemistry, School of Pharmacy, Ardabil University of Medical Sciences, Ardabil, 5618953141, Iran.
E-mail addresses: n.razzaghi@pharmacy.arums.ac.ir, razzaghinima@gmail.com (N. Razzaghi-Asl).

https://doi.org/10.1016/j.molstruc.2018.03.034
0022-2860/

telomerase.

Study of 1,4-benzodioxane containing 1,3,4-oxadiazoles revealed their potentiality for inhibition of telomerase, GSK-3 beta and MetAP pathway [17,18]. Likewise, benztriazol and phenylethanone containing derivatives demonstrated potential FAK inhibitory activity [19,20]. In another study, the inhibitory activity against TS varied with the substituents on different positions of benzene ring joined to 1,3,4-oxadiazole and increased with the incorporation of electron withdrawing groups into the phenyl ring [21].

It seems that pyrrole triazine analogs of 1,3,4-oxadiazole are potential VEGF-2 inhibitors [22,23]. A series of 2,4-bis diphenylamine oxadiazole derivatives have been reported with promising EGFR tyrosine kinase inhibitory activity [24]. Moreover; it was known that inhibition of EGFR signaling not only had an antiproliferative and therapeutic effects but also increased sensitivity to cytotoxic therapies.

In continuation to our interest in structure based design of small molecule heterocyclic structures as potential bioactive compounds, a series of novel cytotoxic1-(5-aryl-1,3,4-oxadiazol-2-yl)-1-(1H-pyrrol-2-yl) methanamines [25] were subjected to combined molecular docking/quantum mechanical (QM) simulations in order to estimate their binding mode/affinity toward several validated chemotherapeutic targets. For more clarification, general procedure of the work is represented schematically (Scheme 1).

2. Materials and methods

2.1. Ligand data set

A series of cytotoxic 1,3,4-oxadizole derivatives (Table 1) were subjected to *in silico* studies [25]. Candidate molecules were checked in terms of Lipinski's rule of five (RO5) [26] and it was revealed that for almost all of the compounds, no deviation from the expected criteria occurred except for compounds **16** and **17** which exhibited a little deviation just in one of their parameters (ClogP 5.24 & 5.51, respectively). Accordingly, the whole candidate ligands could be classified as drug-like structures [26] (Fig. 1).

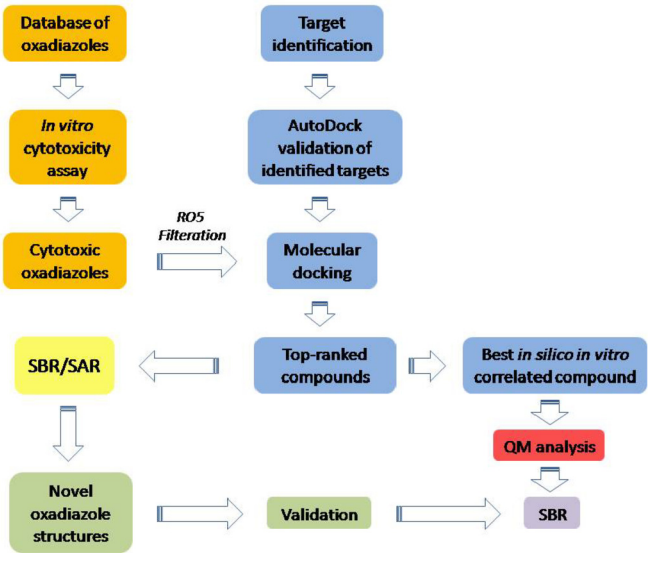

Scheme 1. Schematic flowchart of *in silico* analysis of 1,3,4-oxadiazole derivatives within chemotherapeutic targets.

2.2. Target data set

All radiographic 3D *holo* structures of selected targets (BCL-2, PBD ID: **4AQ3** [27]; EGF, PDB ID: **3W33** [28]; Enoyl-acp Reductase, PDB ID: **1QSG** [29]; FAK, PDB ID: **4KAO** [30]; GSK-3 beta, PDB ID: **1Q41** [31]; HDAC, PDB ID: **5IX0** [32]; MetAP, PDB ID: **1YW7** [33]; telomerase, PDB ID: **5CQG** [34]; TS, PDB ID: **4E5O** [35] and VEGF, PDB ID: **3VO3** [36]) were retrieved from the Brookhaven protein data bank (http://www.rcsb.org/) with resolutions in the range of 1.52–2.40 Å. Macromolecular structures were subjected to optimization step in order to minimize the crystallographic induced bond clashes using steepest descent method. All the pre-processing steps were done by Auto-Dock Tools 1.5.4 (ADT) [37] according to the previous reports [38]. The biological importance of the selected targets with regard to cancer therapy is summarized through separate paragraphs.

2.2.1. Bcl-2

The Bcl-2 family proteins are essential regulators of apoptosis which dictate cellular survival or death decisions by regulating the integrity of the mitochondrial outer membrane (MOM) [39], and include three subgroups of proteins that either promote cell survival (e.g., Bcl-2 and Bcl-x_L), initiate cell killing (e.g., Bcl-2-interacting mediator of cell death (Bim), p53 upregulated mediator of apoptosis (Puma) or Bcl-2-interacting domain (Bid) or activate the effector pathways of apoptosis (Bax, Bak) [40]. As a result, Bcl-2 is an anti-apoptotic protein possessing an important role in various types of cancers like breast which is encoded by the Bcl-2 gene [41].

2.2.2. Epidermal growth factor

Epidermal growth factor (EGF) plays a considerable role in tumor development and progression, including cell proliferation, regulation of apoptotic cell death, angiogenesis and metastatic spread by binding to its receptor, EGFR [42]. Due to the overexpression of EGFR in various types of epithelial cancers, like pancreatic, colorectal, breast, and lung cancer, it has been thought that EGFR is an appropriate target for cancer therapy [43].

2.2.3. Enoyl-acyl carrier protein reductase

Human fatty acid synthase (FAS) is a large, multi-domain protein that synthesizes long chain fatty acids. Human enoyl-acyl carrier protein-reductase (hENR) is one of the FAS catalytic domains, also is the last enzyme in the fatty acid elongation cycle which reduces the substrate enoyl-thioester to an acyl moiety [44]. Because fatty acids are primarily provided by diet, FAS is normally expressed at low levels. However, high levels of FAS expression have been found in many human cancers including breast, prostate, colon, ovary and lung [45].

2.2.4. Focal adhesion kinase

Focal adhesion kinase (FAK) is a cytoplasmic non-receptor tyrosine kinase that is expressed ubiquitously and specifically localized in focal adhesions [46]. Integrin-mediated FAK activation pathway is proven to be involved in survival mechanisms and plays a critical role in the adhesion, invasion, and metastasis of tumor cells [47]. High expressions of FAK have been observed in both endometrial hyperplasia and carcinoma, implying that FAK may play an important role in epithelial-mesenchymal transition (EMT) and migration during endometrial carcinogenesis [48].

2.2.5. Glycogen synthase kinase 3 beta

Glycogen synthase kinase-3 (GSK-3) is a moon-lighting kinase which phosphorylates multiple proteins on serine and threonine residues [49]. The GSK-3 gene family consists of two highly

Table 1
Chemical structures of 1-(5-aryl-1,3,4-oxadiazol-2-yl)-1-(1H-pyrrol-2-yl) methanamines.

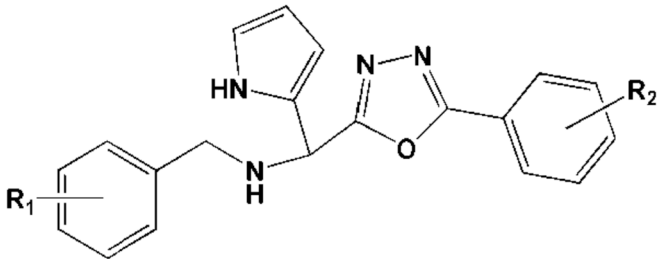

Comp. Code	R_1	R_2	MW	logP	No. HBD[a]	No. HBA[b]	No. RTBs
1	H	H	330.38	3.56	2	5	6
2	H	*m*-Cl	364.83	4.12	2	5	6
3	H	*p*-Cl	364.83	4.12	2	5	6
4	H	3,4-Cl_2	399.27	4.68	2	5	6
5	H	2,4-Cl_2 5-F	417.26	4.84	2	5	6
6	H	*p*-Br	409.28	4.39	2	5	6
7	H	*p*-CH_3	344.41	4.05	2	5	6
8	H	*m*-CH_3	344.41	4.05	2	5	6
9	H	*p*-OCH_3	360.41	3.44	2	6	7
10	H	2,4-$(OCH_3)_2$	390.44	3.31	2	7	8
11	*o*-OCH_3	H	360.41	3.44	2	6	7
12	*p*-OCH_3	H	360.41	3.44	2	6	7
13	*p*-OCH_3	*m*-Cl	394.85	3.99	2	6	7
14	*p*-CH_3	*p*-Br	423.31	4.88	2	5	6
15	*p*-F	*p*-OCH_3	378.4	3.59	2	6	7
16	3,4-Cl_2	*m*-Cl	433.72	5.24	2	5	6
17	3,4-Cl_2	*p*-Br	478.17	5.51	2	5	6

[a] H-bond donor
[b] H-bond acceptor

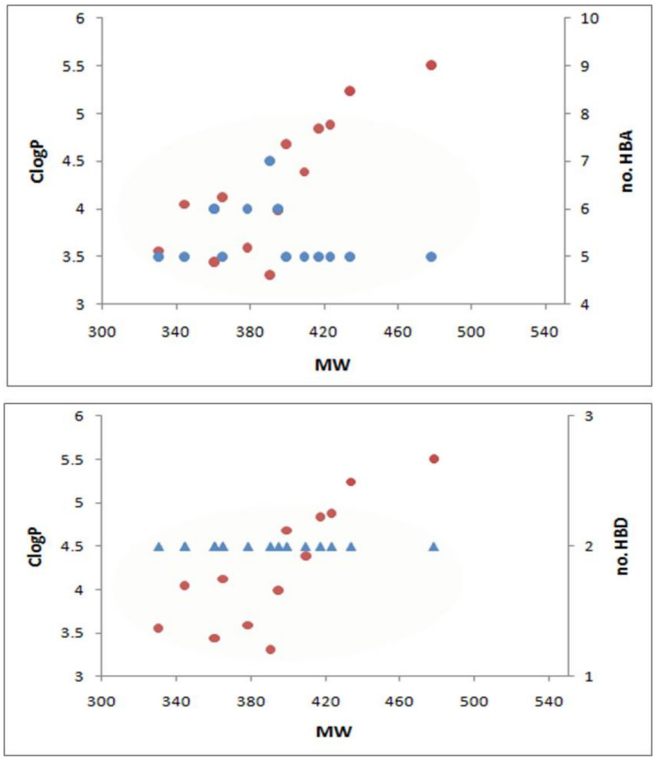

Fig. 1. Distribution patterns of 1-(5-aryl-1,3,4-oxadiazol-2-yl)-1-(1H-pyrrol-2-yl) methanamines with regard to RO5 (red circle: MW *vs* ClogP, blue circle: MW *vs* HBA, blue triangle: MW *vs* HBD).

conserved kinases GSK-3 alpha and GSK-3beta possessing distinct roles. Suppression of GSK-3 beta expression inhibited pancreatic cancer growth and angiogenesis. GSK-3 inhibitors may be appropriate for treatment of tumors exhibiting GSK-3 overexpression in which GSK-3 is acting as a tumor promoter [50].

2.2.6. Histone deacetylase

A common finding in cancer cells is high level expression of HDAC isoenzymes and a corresponding hypoacetylation of histones [51]. HDAC2 expression is elevated in colon cancer cells, possibly as a result of adenomatosis polyposis coli (*APC*) gene deficiency, an early event in colon carcinogenesis [52]. Mutation and/or aberrant expression of various HDACs have often been observed in human disease, in particular cancer, making them important therapeutic targets for many human cancers [53].

2.2.7. Methionine amino peptidase

The methionine aminopeptidases (MetAPs) represent a unique class of proteases. Key active site residues and a dinuclear metal center facilitate the removal of the N-terminal initiator methionine from nascent polypeptides [54]. MetAps initiate co- and post-translational modifications that are essential for the translation, activation, regulation and degradation of proteins in eukaryotic cells [55]. In eukaryotes, there are two genes encoding MetAP, MetAP1 and MetAP2. MetAP2 has attracted much more attention than MetAP1 due to the discovery of MetAP2 as a target molecule of the anti-angiogenic compounds, fumagillin and ovalicin [56]. High expression of MetAP2 has been demonstrated in breast and colorectal cancer [57,58].

2.2.8. Telomerase

Telomerase is a ribonucleoprotein that acts to elongate telomeres in cells that possess its activity. This enzyme is expressed during embryonic development, loses its expression during differentiation of somatic cells, and is almost undetectable in most normal human somatic cells [59]. Telomerase is expressed in more than 85% of human cancer cells and the level of its activity is higher in advanced and metastatic tumors [60]. Thus, it allows cells to escape from the inhibition of cell proliferation due to shortened telomeres. The widespread expression of telomerase in a variety of human cancers, while being almost undetectable in most normal cells, makes it a very attractive drug target [61].

2.2.9. Thymidylate synthase

TS, a homodimer with one active site in each monomer, plays a central role in the biosynthesis of thymidylate, an essential precursor for DNA synthesis and repair. Inhibition of TS disrupts DNA replication, leading to thymine less death in proliferating cells [62]. Ligand-free TS protein binds its own mRNA and thereby represses translation [63]. TS protein and mRNA levels are elevated in many human cancers, and high TS levels have been illustrated in colorectal, breast, cervical, bladder, kidney, and non-small cell lung cancers.

2.2.10. Vascular endothelial growth factor

Vascular endothelial growth factor (VEGF) and its cognate receptor (VEGFR-2) are the most prominent regulators of angiogenesis [64], and are highly expressed in most solid tumors, including prostate cancer. VEGF signaling stimulates cellular pathways that lead to the formation and branching of new tumor blood vessels, promotes rapid tumor growth, and facilitates metastatic potential [65]. Due to the multifaceted effect VEGF has on tumor angiogenesis, tumor cell proliferation, and bone destruction, it has become a rational target for anticancer therapy [66].

2.3. Molecular docking study

Lamarckian genetic algorithm (LGA) of AutoDock 4.2 [67,68] was used to simulate the binding affinity and binding mode of 1,3,4-oxadiazole derivatives in the active site of decuple targets. On the basis of internal validation study, fifty independent genetic algorithm (GA) runs were considered for each ligand under study, except in the case of Bcl-2 for which 100 GA runs were considered. For LGA; 27000 maximum generations; a gene mutation rate of 0.02; and a crossover rate of 0.8 were applied. AutoGrid was used to estimate the grid maps of the protein. For this purpose, on the basis of the volumes of candidate molecules, a grid of $40 \times 40 \times 40$ points in x, y, and z directions was built centered on the center of mass of the catalytic site of intended co-crystallographic ligands (spacing: 0.375 Å). Cluster analysis was performed on the docked results using a root mean square deviation (RMSD) threshold of 2 Å. The best docking result in each case was considered to be the conformation with the lowest binding energy. Schematic 2D representations of the ligand-receptor interactions were recorded by LIGPLOT [69].

2.4. QM simulation

Simulated amino acid residues were considered on the basis of detected interacted components of docked top-ranked oxadiazole compounds. To mimic the real electronic state of all involved residues, *N*-terminals and C-terminals were acetylated and methyl amidated respectively to imitate the original electron density. Due to the unclear position of H-bonds in a typical X-ray crystallographic file, we further optimized the heavy atom/H-bonds by the same method and basis set using heavy atom fixing approximation method (constrained optimizations) [70]. All the interaction energies were estimated through functional B3LYP associated with split valence basis set using polarization functions (Def2-SVP) incorporated into ORCA quantum chemistry package [71].

3. Results and discussion

3.1. Molecular docking

Available X-ray crystallographic data on Protein Data Bank (PDB) simplified the structure based design of desired enzyme inhibitors by docking simulation which is a key tool in structural molecular biology and computer-assisted drug design (CADD) [72]. Numerous successful applications of molecular docking in drug discovery efforts have been reported [73]. AutoDock is well established docking software which has offered several fruitful advantages in designing bioactive compounds (http://autodock.scripps.edu) [74].

3.1.1. Internal validation

The validity of the method was interpreted in terms of RMSD of the ligand atoms in the re-docked and crystallographic conformations [75] (Table 2). For comparison purposes, crystallographic and docked poses of ligands are depicted in Fig. 2.

3.1.2. Estimated binding affinities & in silico in vitro correlation

To calculate the binding affinities of 1,3,4-oxadiazoles (**1**–**17**) toward selected targets, all the ligand structures were docked into the active site of desired receptors. In all simulations, it was assured that top-ranked docking outputs were supported by high cluster populations. Results are summarized in Table 3. Besides free binding energy, to consider compounds that use their atoms more efficiently in binding to target, ligand efficiency (LE) indices which are indicative of binding affinity with regard to number of heavy atoms [76] were also estimated via Eq. (1) in which HAC stands for

Table 2
AutoDock 4.2 validation results for different *holo* PDB structures of intended chemotherapeutic targets.

No.	Target	PDB ID	Resolution of PDB structure (Å)	Estimated K_i(μM)	RMSD from Reference (Å)	No. GA runs	No. conformations in top-ranked cluster	Max. No. energy eval.
1	Bcl-2	4AQ3	2.40	7.68×10^{-4}	1.68	100	23	3×10^{6}
2	EGF	3W33	1.70	3.58×10^{-4}	0.74	50	30	2.5×10^{6}
3	ENR	1QSG	1.75	0.348	0.36	50	50	2.5×10^{6}
4	FAK	4KAO	2.39	3.61×10^{-4}	0.49	50	50	2.5×10^{6}
5	GSK-3 beta	1Q41	2.10	0.0851	0.47	50	50	2.5×10^{6}
6	HDAC	5IX0	1.72	0.008	0.86	50	50	2.5×10^{6}
7	MetAP	1YW7	1.85	15.40	0.74	50	40	2.5×10^{6}
8	Telomerase	5CQG	2.30	0.015	0.94	50	19	2.5×10^{6}
9	TS	4E5O	1.70	4.07	0.56	50	19	2.5×10^{6}
10	VEGF	3VO3	1.52	2.50×10^{-4}	0.49	50	21	2.5×10^{6}

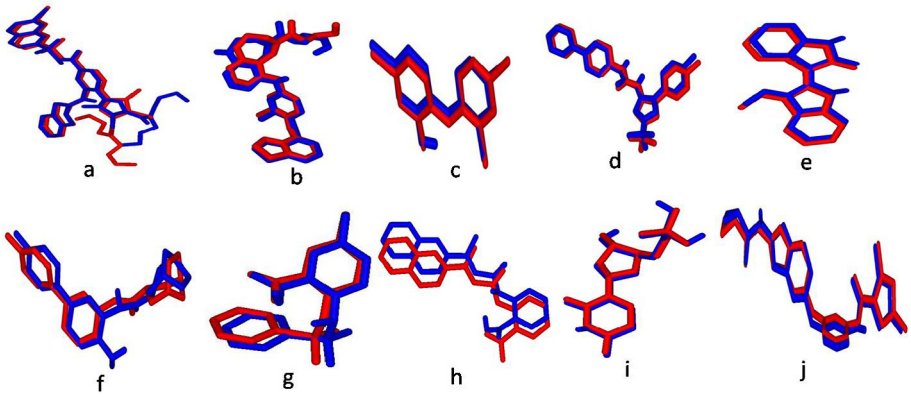

Fig. 2. Binding poses of cognate ligands within active site of relevant targets in docked ( ) and crystallographic ( ) states; **a)** Bcl-2, RMSD 1.68 Å, **b)** EGF, RMSD 0.74 Å, **c)** ENR, RMSD 0.36 Å, **d)** FAK, RMSD 0.49 Å, **e)** GSK-3 beta, RMSD 0.47 Å, **f)** HDAC, RMSD 0.86 Å, **g)** MetAP, RMSD 0.74 Å, **h)** Telomerase, RMSD 0.94 Å, **i)** TS, RMSD 0.56 Å, **j)** VEGF, RMSD 0.49 Å.

Table 3
Docking simulation results of oxadiazoles against chemotherapeutic targets (HAC: heavy atom count; LE: ligand efficiency)

Ligand code	HAC	BCL-2			EGF			ENR			FAK			GSK-3 beta		
		K_i (μM)	ΔG_b (kcal/mol)	LE	K_i (μM)	ΔG_b (kcal/mol)	LE	K_i (μM)	ΔG_b (kcal/mol)	LE	K_i (μM)	ΔG_b (kcal/mol)	LE	K_i (μM)	ΔG_b (kcal/mol)	LE
1	25	16.50	−6.52	0.26	0.152	−9.30	0.37	0.094	−5.50	0.22	0.079	−9.69	0.39	0.394	−8.74	0.35
2	26	14.17	−6.61	0.25	0.057	−9.88	0.38	0.001	−8.08	0.31	0.153	−9.30	0.36	0.221	−9.08	0.35
3	26	11.75	−6.73	0.26	0.051	−9.94	0.38	0.685	−8.41	0.32	0.156	−9.29	0.36	0.171	−8.32	0.32
4	27	3.66	−7.42	0.27	0.017	−10.59	0.39	0.115	−9.46	0.35	0.056	−9.90	0.37	0.497	−9.96	0.37
5	28	7.78	−6.97	0.25	0.028	−10.31	0.37	0.238	−9.04	0.32	0.114	−9.47	0.34	1.04	−8.16	0.29
6	26	10.81	−6.78	0.26	0.035	−10.18	0.39	0.241	−9.03	0.35	0.104	−9.52	0.37	0.064	−9.81	0.38
7	26	18.97	−6.44	0.25	0.066	−9.79	0.38	0.447	−8.66	0.33	0.196	−9.15	0.35	0.144	−9.33	0.36
8	26	7.45	−7.00	0.27	0.072	−9.75	0.36	0.554	−8.54	0.33	0.047	−10.00	0.38	0.296	−8.91	0.34
9	27	18.78	−6.45	0.24	0.066	−9.80	0.36	0.318	−8.86	0.33	0.282	−8.94	0.33	0.141	−9.35	0.35
10	29	13.25	−6.65	0.23	0.052	−9.93	0.34	0.991	−8.19	0.28	0.185	−9.19	0.32	0.213	−9.10	0.31
11	27	15.86	−6.55	0.24	0.061	−9.84	0.36	0.461	−8.64	0.32	0.106	−9.51	0.35	0.950	−8.22	0.30
12	27	10.32	−6.80	0.25	0.174	−9.22	0.34	0.397	−8.73	0.32	0.028	−10.30	0.38	1.45	−8.44	0.31
13	28	10.19	−6.81	0.24	0.111	−9.49	0.34	0.609	−8.48	0.30	0.129	−9.40	0.34	0.581	−8.51	0.30
14	27	7.53	−6.99	0.26	0.017	−10.60	0.39	0.484	−8.61	0.32	0.124	−9.44	0.35	0.470	−9.66	0.36
15	28	24.70	−6.29	0.24	0.078	−9.70	0.35	0.001	−8.17	0.29	0.311	−8.88	0.32	1.21	−8.07	0.29
16	28	3.07	−7.52	0.27	0.013	−10.74	0.38	0.322	−8.86	0.32	0.058	−9.87	0.35	0.136	−9.37	0.33
17	28	1.52	−7.92	0.28	0.008	−11.06	0.4	0.227	−9.06	0.32	0.062	−9.84	0.35	0.153	−10.30	0.37

Ligand code	**HAC**	HDAC			MetAP			Telomerase			TS			VEGF		
		K_i (μM)	ΔG_b (kcal/mol)	LE	K_i (μM)	ΔG_b (kcal/mol)	LE	K_i (μM)	ΔG_b (kcal/mol)	LE	K_i (μM)	ΔG_b (kcal/mol)	LE	K_i (μM)	ΔG_b (kcal/mol)	LE
1	25	2.88	−7.56	0.36	0.003	−11.71	0.47	6.00	−7.12	0.28	0.604	−8.48	0.34	0.026	−10.33	0.41
2	26	0.99	−8.19	0.37	7.98×10^{-4}	−12.41	0.48	5.39	−7.19	0.28	0.581	−8.51	0.33	0.042	−10.07	0.39
3	26	1.03	−8.17	0.37	5.34×10^{-4}	−12.65	0.49	3.39	−7.46	0.29	1.15	−8.10	0.31	0.010	−10.91	0.42
4	27	0.48	−8.62	0.39	5.30×10^{-4}	−12.65	0.47	2.13	−7.74	0.29	1.17	−8.09	0.30	0.004	−11.39	0.42
5	28	0.698	−8.40	0.35	0.002	−11.97	0.43	1.91	−7.80	0.28	0.882	−8.26	0.30	0.054	−9.91	0.35
6	26	0.688	−8.41	0.40	7.23×10^{-4}	−12.47	0.48	3.10	−7.51	0.29	1.12	−8.12	0.31	0.018	−10.56	0.41
7	26	1.36	−8.01	0.37	8.03×10^{-4}	−12.41	0.48	5.39	−7.19	0.28	1.52	−7.94	0.30	0.012	−10.79	0.42
8	26	1.09	−8.14	0.38	0.001	−12.27	0.47	5.37	−7.19	0.28	0.736	−8.37	0.32	0.043	−10.05	0.39
9	27	1.95	−7.79	0.36	0.001	−12.13	0.45	5.26	−7.20	0.27	0.968	−8.20	0.30	0.022	−10.46	0.39
10	29	1.86	−7.82	0.31	0.006	−11.20	0.39	4.44	−7.30	0.25	1.17	−8.09	0.28	0.058	−9.87	0.34
11	27	3.41	−7.46	0.35	0.002	−11.88	0.44	5.26	−7.20	0.27	0.988	−8.19	0.30	0.092	−9.60	0.36
12	27	0.965	−8.21	0.34	0.001	−12.09	0.45	4.65	−7.28	0.27	0.746	−8.36	0.31	0.090	−9.61	0.36
13	28	0.562	−8.53	0.36	5.69×10^{-4}	−12.61	0.45	2.22	−7.71	0.28	0.539	−8.55	0.30	0.081	−9.67	0.34
14	27	0.523	−8.57	0.38	3.39×10^{-4}	−12.92	0.48	1.94	−7.79	0.29	1.05	−8.15	0.30	0.046	−10.01	0.37
15	28	2.30	−7.69	0.34	0.002	−11.81	0.42	8.77	−6.90	0.25	0.937	−8.22	0.29	0.132	−9.39	0.34
16	28	0.483	−8.62	0.38	7.94×10^{-4}	−12.41	0.44	1.66	−7.88	0.28	0.634	−8.46	0.30	0.024	−10.40	0.37
17	28	0.391	−8.74	0.38	3.57×10^{-4}	−12.89	0.46	1.33	−8.01	0.29	0.482	−8.62	0.31	0.016	−10.61	0.38

heavy atom counts (a number of non-hydrogen atoms) of a ligand.

$$LE = -\frac{\Delta G_b}{HAC} \quad (1)$$

It should be noticed that cytotoxic effects of selected compounds were previously evaluated *in vitro* by the MTT (3-(4,5-dimethylthiazol-2-yl)-2,5-diphenyltetrazolium bromide) assay against A549 (human alveolar basal epithelial adenocarcinoma), HT29 (human colorectal adenocarcinoma), HT1080 (human fibrosarcoma) and MCF-7 (human breast adenocarcinoma) cell lines [25].

AutoDock driven binding affinities in terms of ΔG_b, k_i and LE were subjected to linear regression analysis *vs in vitro* cytotoxic activities [25] to find a most satisfying model. On the basis of acquired data, relatively adaptable correlation could just be achieved

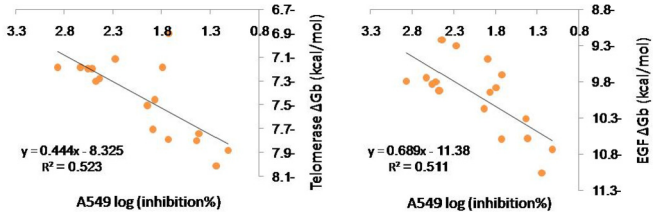

Fig. 3. Correlation curve between experimentally determined log(inhibition%) and estimated binding affinities toward telomerase and EGF for 1,3,4-oxadiazole derivatives.

in the case of telomerase ($R^2 = 0.52$) and EGF ($R^2 = 0.51$) complexes (Fig. 3) within A549 cell line. It is proposed that blocking telomerase and EGF might be further exploited as possible mechanism for cytotoxic activity of 1,3,4-oxadiazoles in adenocarcinoma human alveolar basal epithelial cancer cells (A549). Subsequent targets which exhibited intermediate correlations were HDAC and Bcl-2 with regression coefficients of 0.47 and 0.45, respectively.

In the case of Bcl-2, EGF, ENR, FAK, GSK-3 beta, telomerase, and VEGF, it was found interestingly that docked top-ranked ligand also exhibited highest LE (independently or along with another molecule). However, in the case of HDAC, MetAP, and TS, compounds possessing superior LE values (**6**, **3**, and **1,** respectively) were not necessarily the ones with top-ranked binding energies (**17**, **14**, and **17**). Such observation emphasized that within Bcl-2, EGF, ENR, FAK, GSK-3 beta, telomerase, and VEGF, there might be a good correlation between the estimated affinity and corrected affinity of molecules with regard to their size.

Careful comparison of ΔG_b values among different targets (Table 3) demonstrated that binding affinity of ligands toward MetAP was superior to the other targets (−11.20 to −12.92 kcal/mol). However, MetAP could not exert this preferential affinity when correlated with different cell line IC_{50} values.

3.2. Structure binding relationship (SBR)

Binding characteristics of the top-ranked 1,3.4-oxadiaoles within each interacted target is summarized in Table 4.

Considering various R_1 and R_2 substituents within general structure of oxadiazole compounds (Table 1), binding models differed among docked ligands and regarding the results, following SBRs were rationalized:

- It was previously revealed that incorporation of halogen atoms in 5-substituted phenyl ring and *N*-benzyl moieties improved the cytotoxic activity against A549, HT29, HT1080 and MCF-7 cell lines [25]. Interestingly such observation was in accordance with new findings in a way that compounds **4** and **17** were top-ranked ligands in two and six of the docked targets, respectively (Table 4).
- Unlike compound **4** that bears 3,4-dichloro substituent, compound **5** with varied substitution pattern (2,4-dichloro-5-flouro) was recognized as false negative in modeling simulations, since it previously exhibited good cytotoxic effects against A549, HT29, HT1080 and MCF-7 cell lines [25].
- Comparison of ΔG_b for compounds **16** and **17** (Table 3) pointed that 3,4-dichloro benzyl group provided increased inhibitory activity against Bcl-2, telomerase and HDAC.
- Interaction models showed that secondary benzyl amine, pyrrole NH, and N3 of oxadiazole ring participated in H-bond interactions within various docked targets. It was also found that oxygen and N4 atoms of oxadiazole ring had a little participation in H-bond interactions with the residues of desired targets.
- In the case of GSK-3 beta, the key residue participated in H-bond interaction with all ligands was Val135. Accordingly, Tyr67 (Bcl-2), Asp855 (EGF), Ser91 (ENR), Glu471 (FAK), Gly154 (HDAC), His231 (MetAP), Phe494 (telomerase), His190 and Asn220 (TS, and Glu885) and Asp1046 (VEGF) were recognized as key residues involved in H-bond interactions.
- Participation of pyrrole ring in H-bond interactions with Bcl-2 (Tyr76), telomerase (Phe494), HDAC (His145), GSK-3 beta (Ile62), MetAP (Asn329), TS (His190) and VEGF (Val899) demonstrated that it could be chosen as an important inhibitory moiety against mentioned targets. Results of previous inhibitory structures [10] and also H-bond interaction characteristics (Table 4) were in agreement with this rationalization.
- For comparison purposes, Autodock driven free binding energies for top-ranked ligands were compared to that of co-crystallographic ones (Table 5). As can be seen from the data, top-ranked oxadiazole molecules exhibited superior binding affinities than co-crystallographic ligands toward ENR, GSK-3 beta, MetAP and TS.

3.3. SAR/SBR refreshment

On the basis of estimated docking results and previously studied 2,5-disubstituted 1,3,4-oxadiazoles with relatively good cytotoxic activity [10], following schematic SAR/SBR for candidate oxadiazoles was offered (Fig. 4).

In general, the cytotoxic activity of 1,3,4-oxadiazole derivatives seemed to be dependent on the nature of the substituent rather the core skeleton of the molecule. However, H-bond interaction patterns of targets under study clarified that depending on the anticancer target, 1,3,4-oxadiazole nucleus can blurt cytotoxic activity. Regarding the structures of best docked ligands and their important interacting groups, a series of 1,3,4-oxadiazole derivatives were proposed (Fig. 5) and validated via docking into the mostly inhibited targets (Bcl-2, EGF, HDAC, MetAP and telomerase). Rationales behind designation of the proposed compounds were as follows:

- According to the importance of substituents adjacent to 1,3,4-oxadiazole nucleus and re-checking the best docked structures (**4** and **17**), 3,4-dichloro substituted phenyl rings (R_1 and R_2) were incorporated into the proposed structures (Fig. 6: **a**-**d**). This incorporation is schematically depicted in Fig. 5 (see Figs. 7 and 9).
- Inclusion of sulfide linkage is due to its recognition in the structure of the majority of the previously EGF and telomerase inhibitors [10]. Moreover; it has also been reported that sulfur is an important atom for TS inhibition (Fig. 6: **a-c**) [10].
- Due to the previous studies on HDAC inhibitors, Zn^{2+} binding group along with linker and surface recognition moiety were required for efficient inhibition of HDAC [10]. For this purpose, Zn^{2+} binding hydroxamate group was added to the proposed structures (Fig. 6: **a** and **b**).
- To mimic the amino oxadiazole moiety in previously reported derivatives [77], carbon atom between amine group and 1,3,4-oxadiazole heterocycle was moved to the proximity of pyrrole ring to propose a new HDAC inhibitor with aminopyrrole moiety as a new linker to both surface recognition cap and zinc binding group (Fig. 6: **b**, **c** and **d**).

Table 4
Hydrophobic and H-bond interaction characteristics for docked oxadiazole derivatives into the active site of chemotherapeutic targets.

Target	PDB code	Best docked ligand code	Estimated K_i (μM)	Residues involved in hydrophobic contacts	Residues involved in H-bonds	H-bond distances (Å)[a]	Atoms of ligand involved in H-bonds	Atoms of residue involved in H-bonds
Bcl-2	4AQ3	17	1.520	Phe63, Tyr67 Asp70, Phe71 Met74, Glu95 Leu96, Arg98 Asp99, Arg105 Phe112	Tyr67	2.84	NH (pyrrole)	OH (side chain hydroxyl)
EGF	3W33	17	0.008	Leu718, Val726 Ala743, Lys745 Met766, Cys775 Arg776, Leu777 Leu788, Thr790 Thr854, Asp855 Phe856	Asp855 Asp855 Thr854	2.92 2.98 3.01	NH (amine) N3 (oxadiazole) NH (amine)	O (side chain carboxylate) O (side chain carboxylate) C=O (backbone)
ENR	1QSG	4	0.115	Gly13, Ala15 Ser19, Ile20 Ser91, Ile92 Gly93, Leu144 Tyr146, Lys163 Ala189, Gly190 Pro191, Ile192 Thr194, Leu195 Ala196, Ala197 Phe203	Ser91 Ser91 Ser91	2.78 2.97 3.05	NH (amine) NH (amine) NH (amine)	C=O (backbone) C=O (backbone) C=O (backbone)
FAK	4KAO	12	0.047	Val436, Ala452 Lys454, Glu471 Thr474, Met475 Phe478, Val484 Met499, Gly563 Asp564, Phe565	Asp564 Glu471	2.75 3.24	NH (amine) NH (amine)	C=O (backbone) O (side chain carboxylate)
GSK-3 beta	1Q41	17	0.153	Ile62, Ala83 Val110, Leu132 Asp133, Tyr134 Val135, Pro136 Thr138, Arg141 Leu188, Cys199	Val135 Val135 Ile62	2.64 2.78 2.98	NH (amine) N3 (oxadiazole) NH (pyrrole)	C=O (backbone) C=O (backbone) C=O (backbone)
HDAC	5IX0	17	0.391	Met35, Asp104, Leu144,His146 Gly154, Phe155 Cys156, Asp181 His183, Asp186, Tyr209, Phe210 Asp269, Leu276 Gly305, Gly306 Tyr308	His146	2.68	N2 (oxadiazole)	NH (side chain imidazole)
MetAP	1YW7	14	0.003	Phe219, Pro220 His231, Asp251 Asp262, Leu328 Asn329, His331 Ile338, Glu364 His382, Tyr383 Met384, Ala414 Tyr444, Glu459	Asn329 Glu364 His231	2.75 2.77 3.14	NH (pyrrole) NH (amine) O (oxadiazole)	C=O (backbone) O (side chain carboxylate) NH (side chain imidazole)
Telomerase	5CQG	17	1.330	Met482, Met483 Arg486, Asp493 Phe494, Gly495 Ile497, Trp498 Ile550, Tyr551 Leu554, Arg557	Phe494	2.69	NH (pyrrole)	C=O(backbone)
TS	4E5O	17	0.482	Glu81, Ile102 Trp103, Tyr129 Cys189, His190 Gln208, Ser210, Gly211, Asp212 Gly216, Phe219 Asn220, His250	Glu81 His190 Asn220	2.68 3.03 3.27	NH (amine) NH (pyrrole) O (oxadiazole)	O (side chain carboxylate) NH (side chain imidazole) NH (side chain amine)
VEGF	3VO3	4	0.004	Leu840, Val848 Val867, Lys868 Ala866, Glu885 Leu889, Val898 Val899, Val914 Val916, Glu917 Phe918, Leu1035 Ile1044, Cys1045 Asp1046, Phe1047	Glu885 Asp1046 Val899	2.59 2.88 2.96	NH (amine) N3 (oxadiazole) NH (pyrrole)	O (side chain carboxylate) C=O (backbone) C=O (backbone)

[a] H-bond distances are reported as (H … acceptor) lengths.

Table 5
Simulation results for superior docked ligands into the active site of chemotherapeutic targets.

Target	PDB code	Best docked ligand code	ΔG_b (kcal/mol) docked ligand	ΔG_b (kcal/mol) cognate ligand
Bcl-2	4AQ3	17	−7.92	−12.43
EGF	3W33	17	−11.06	−12.89
ENR	1QSG	4	−9.46	−8.81
FAK	4KAO	12	−10.30	−12.88
GSK-3 beta	1Q41	17	−10.30	−9.65
HDAC	5IX0	17	−8.74	−11.04
MetAP	1YW7	14	−12.92	−6.57
Telomerase	5CQG	17	−8.01	−10.69
TS	4E5O	17	−8.62	−7.35
VEGF	3VO3	4	−11.39	−13.10

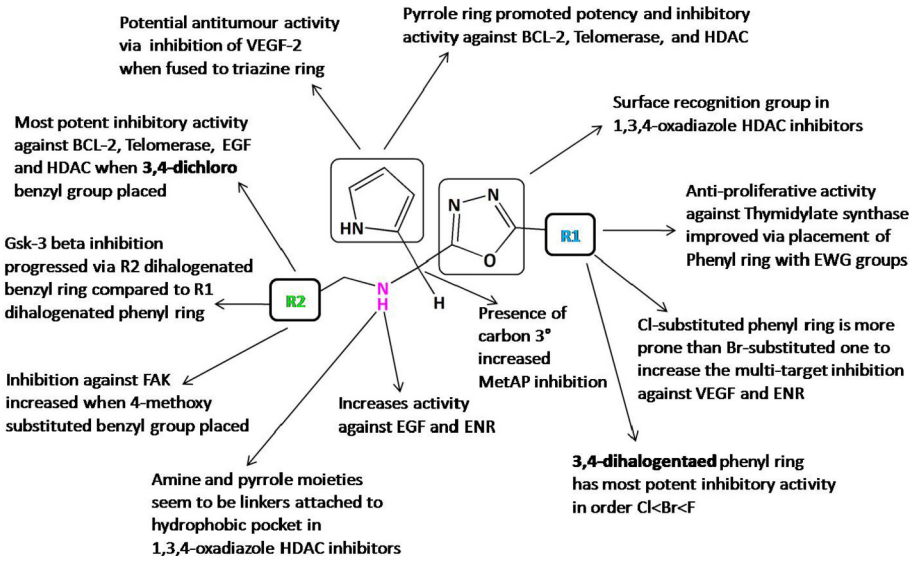

Fig. 4. Schematic representation of SAR/SBR for 1-(5-aryl-1,3,4-oxadiazol-2-yl)-1-(1H-pyrrol-2-yl) methanamines toward chemotherapeutic targets.

- Previous studies revealed that 1,4-benzodioxane containing oxadiazoles were efficient telomerase, GSK-3 beta and MetAP inhibitors [10]. Accordingly, a dioxane ring was fused to the benzyl group and two Cl atoms were moved to the dioxane ring. This possible solution led to the designation of compound **e** (Fig. 6: **e**).

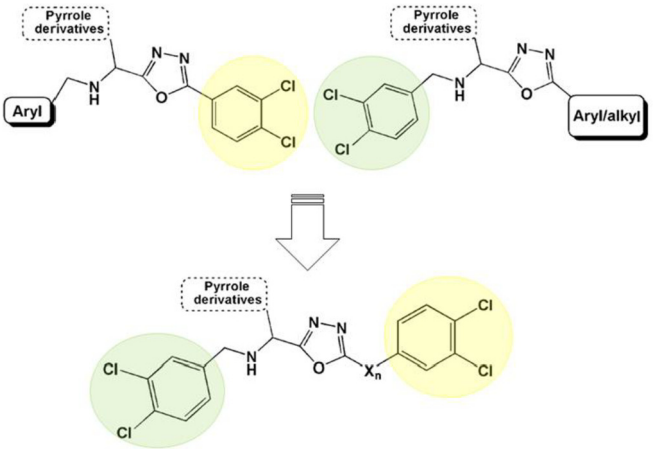

Fig. 5. Incorporating different aryl scaffolds of 1,3,4-oxadiazoles into a hybrid structure.

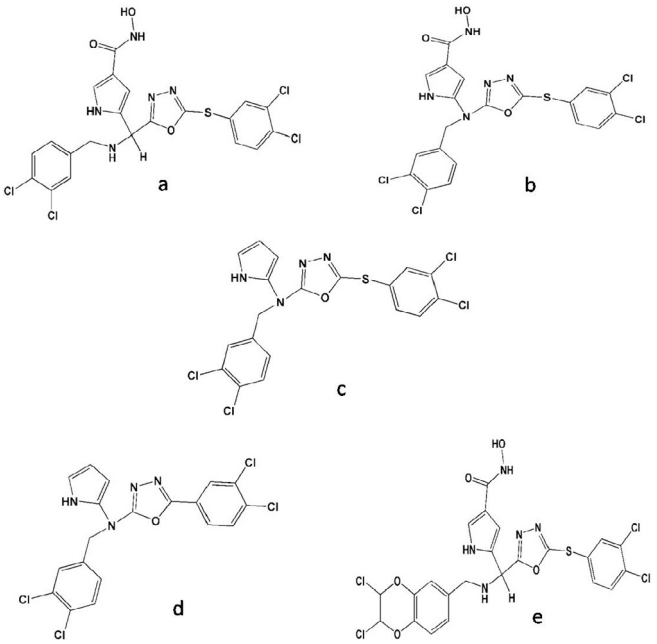

Fig. 6. Chemical structures of the proposed 1,3,4-oxadiazole derivatives with potential multi-chemotherapeutic target inhibitory activities.

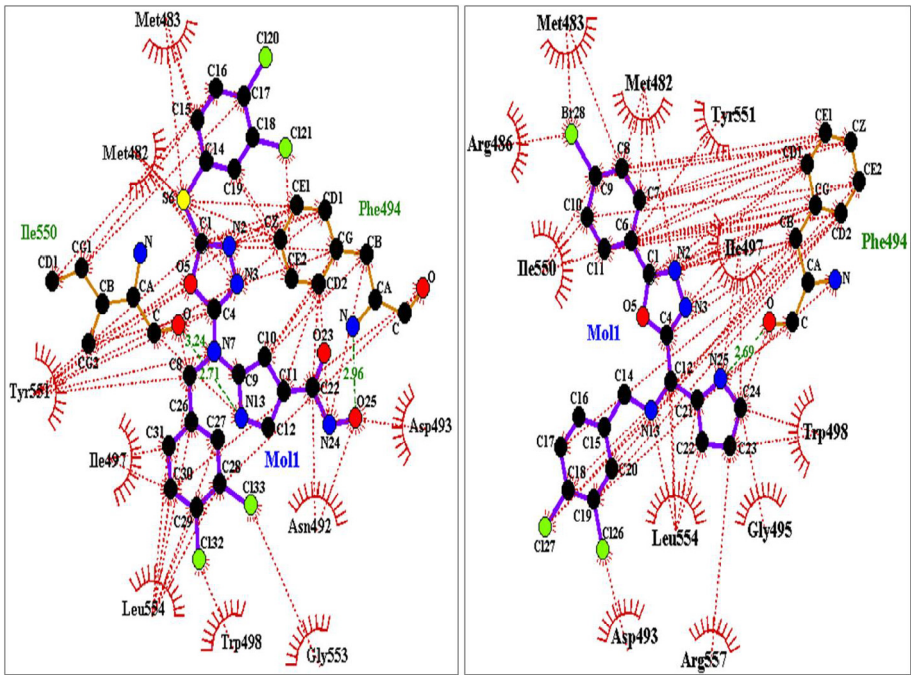

Fig. 7. 2D scheme of binding interactions between proposed compound **b** (left)/best docked ligand (right) and telomerase (PDB ID: **5CQG**) generated by LIGPLOT.

3.4. Validation study

Compounds **a**-**e** were docked into the active sites of desired macromolecules (Bcl-2, EGF, HDAC and telomerase). Comparing ΔG_b values of proposed and best docked ligands for each target demonstrated that compounds **a** and **b** exhibited better binding ability within all quadruple targets (Table 6). Since MetAP exhibited a noticeable superiority in terms of ΔG_b values among all targets (*refer to* Table 3), we supposed to dock these ligands into the MetAP as well. Results showed that except compounds **a** and **e**, three other molecules exhibited weaker binding affinities toward MetAP when compared to top-ranked docked ligand (Table 6). Moreover; modeling study might not support the important role of Zn^{2+} binding hydroxamate since binding affinity of compound **c** (−9.61 kcal/mol) was not so different with that of **a** and **b** (−9.65 & −9.53 kcal/mol).

Compounds **a**, **b** and **e** exhibited superior docking results within intended targets. However, we can signify the spectacular role of **a** regarding its enhanced inhibitory activity against all quintet targets. Beside compound **a**, interestingly, compounds **b** and **e** were the forefront molecules in affinity ranking due to their relatively lower ΔG_b values within targets (except **b** toward MetAP and **e** toward HDAC). Due to the superiority of b in binding to telomerase, 2D schematic representation of binding interactions are depicted in Fig. 8.

Results of docking compound **e** into the active site of Bcl-2, EGF, HDAC, MetAP and telomerase confirmed our assumption since better ΔG_b values were achieved in all targets except HDAC (Table 6). Due to the inhibition of GSK-3 beta by 1,4-benzodioxane substituted oxadiazoles [10], compound **e** was docked into the active site of GSK-3 beta as well and superior ΔG_b values affirmed our designation (ΔG_b for best docked ligand and proposed ligand were −10.30 and −11.01 kcal/mol, respectively). Designation of a 1,4-benzodioxan containing oxadiazole (**e**) resulted in considerable increase in binding affinities toward assessed targets, except HDAC (Table 6). Moreover, oxygen atoms of dioxane ring and its 2,3-dichloro substituent participated in H-bond and electrostatic interactions, respectively (Fig. 8)

3.4.1. Effect of sulfur linkage

It was primarily supposed that incorporation of sulfide linkage might enhance the binding ability of oxadiazoles via possible hydrophobic interactions. Since the mere structural difference of compounds **c** and **d** was attributed to the presence of sulfur moiety in **c** (Fig. 6), comparative evaluation of intermolecular binding interactions might be informative. At first glance, results of Table 6 showed that within Bcl-2 and HDAC, sulfur containing molecule (**c**) was identified as weaker binder while in the case of MetAP and telomerase, it seemed that sulfur linkage enhanced the binding capability. Moreover; compounds **c** and **d** did not show any

Table 6
Binding affinity of proposed oxadiazole structures and best docked oxadiazoles *vs* selected chemotherapeutic targets.

Comp. code	Bcl-2		EGF		HDAC		MetAP		Telomerase	
	ΔG_b[a] best docked ligand (kcal/mol)	ΔG_b proposed ligand (kcal/mol)	ΔG_b best docked ligand (kcal/mol)	ΔG_b proposed ligand (kcal/mol)	ΔG_b best docked ligand (kcal/mol)	ΔG_b proposed ligand (kcal/mol)	ΔG_b best docked ligand (kcal/mol)	ΔG_b proposed ligand (kcal/mol)	ΔG_b best docked ligand (kcal/mol)	ΔG_b proposed ligand (kcal/mol)
a	−7.92	−8.30	−11.06	−11.30	−8.74	−9.65	−12.92	−13.40	−8.01	−9.35
b	−7.92	−8.24	−11.06	−12.27	−8.74	−9.53	−12.92	−10.91	−8.01	−11.47
c	−7.92	−7.49	−11.06	−10.78	−8.74	−9.61	−12.92	−9.99	−8.01	−10.05
d	−7.92	−7.84	−11.06	−10.74	−8.74	−10.09	−12.92	−9.56	−8.01	−9.68
e	−7.92	−8.48	−11.06	−12.25	−8.74	−8.11	−12.92	−14.35	−8.01	−10.41

[a] ΔG_b values were introduced form Table 5.

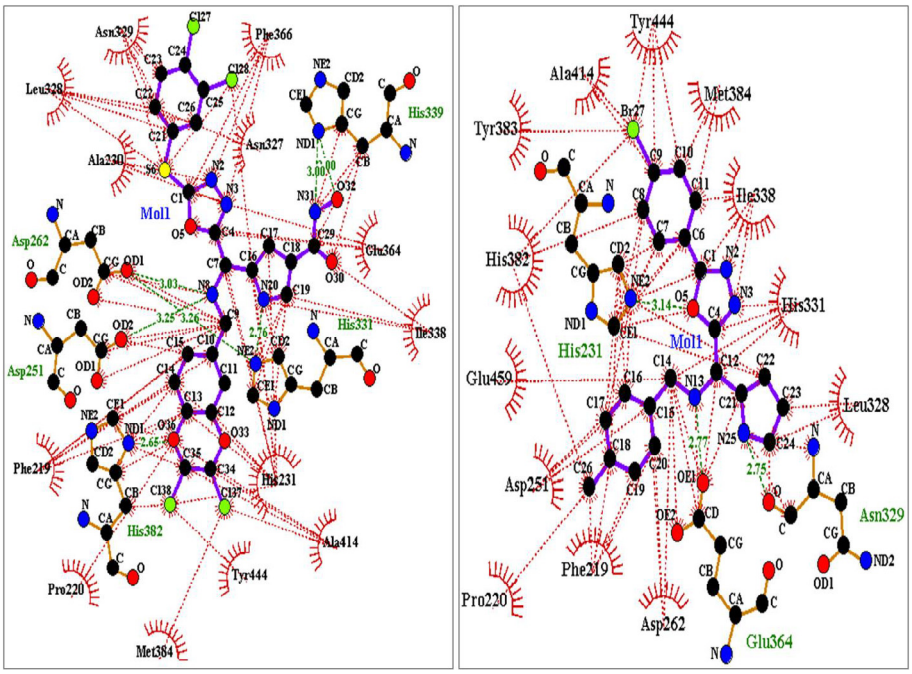

Fig. 8. 2D scheme of binding interactions between proposed compound **e** (left)/best docked ligand (right) and MetAP (PDB ID: **1YW7**) generated by LIGPLOT.

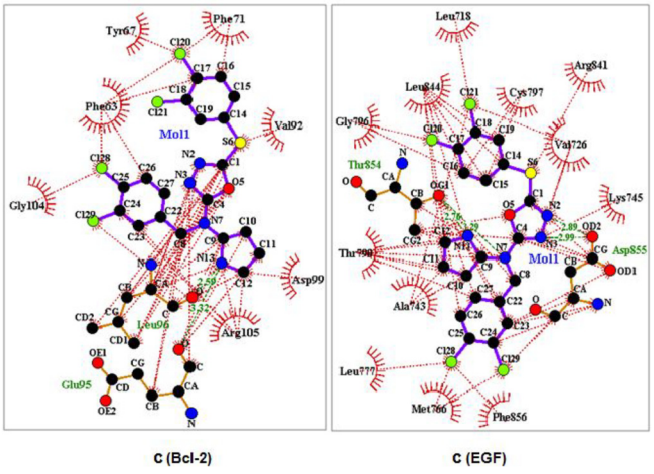

Fig. 9. 2D scheme of binding interactions between proposed compound **c**, Bcl-2 (PDB ID: **4AQ3**) and EGF (PDB ID: **3W33**) generated by LIGPLOT.

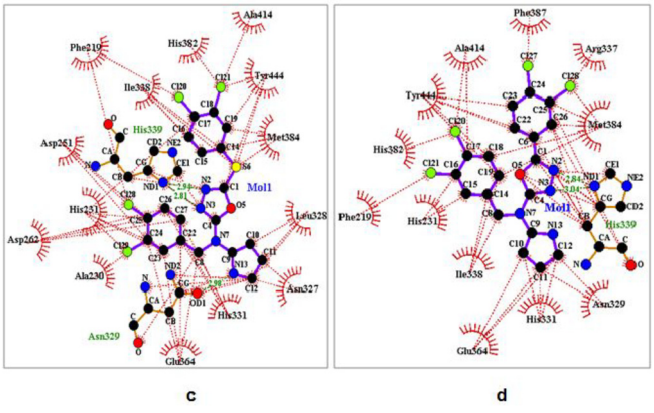

Fig. 10. 2D scheme of binding interactions between proposed compound **c** and MetAP (PDB ID: **1YW7**) generated by LIGPLOT.

meaningful difference in binding toward EGF.

To further elucidate the above observations, 2D schematic binding models of designated ligands were depicted in Figs. 10–12. Within Bcl-2 and EGF active sites, sulfur atom participated in just one hydrophobic contact with Val92 (Bcl-2) and Arg841 (EGF) but careful inspection of Figs. 10 and 11 revealed more hydrophobic contacts for sulfur atom. This was possibly in accordance with obtained binding energy values (*refer to* Table 6) and emphasized on important role of sulfur linkage in making efficient lipophilic interactions.

3.4.2. Zn^{2+} binding moiety

According to the importance of Zn^{2+} cofactor in ligand/receptor interactions within HDAC active site, binding interactions between

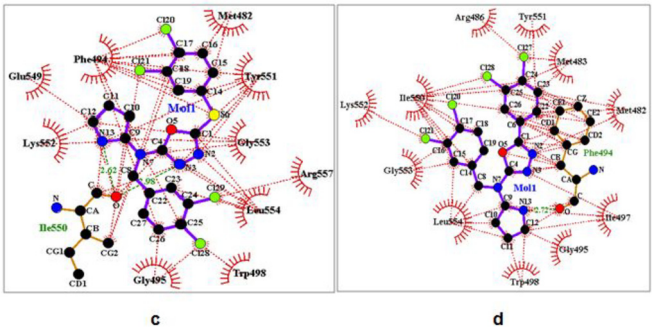

Fig. 11. 2D scheme of binding interactions between proposed compound **c** and telomerase (PDB ID: **5CQG**) generated by LIGPLOT.

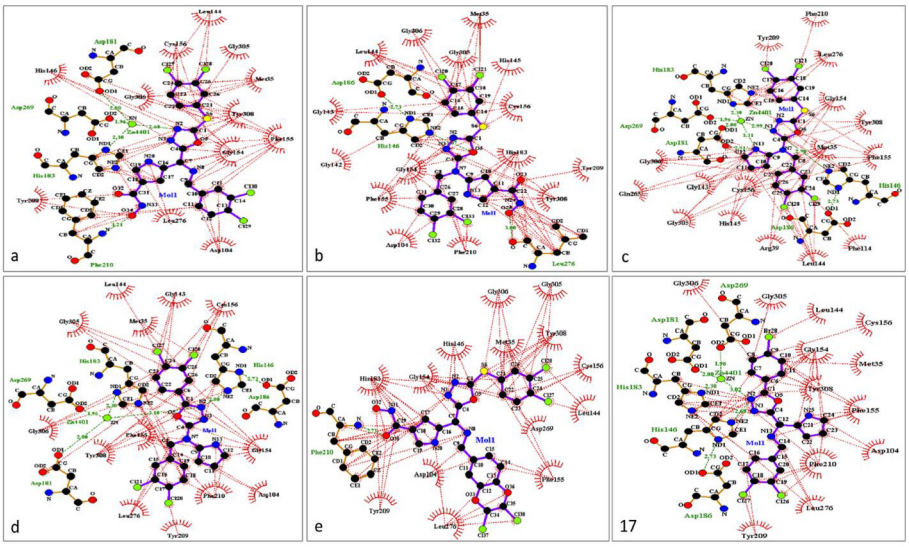

Fig. 12. Binding interaction comparison of docked oxadiazole compounds (**a**–**e**) into HDAC active site (PDB ID: **5IX0**).

Zn^{2+} and docked compounds were explored separately in our study. Moreover, oxadiazole nucleus was previously introduced as a surface recognition group for HDAC inhibition [10,15] (Fig. 4). In this regard, schematic binding patterns of **17** within HDAC active site represented that oxadiazole N2 atom participated in *pseudo cation-π* interaction with Zn^{2+} cofactor (bond distance 3.02 Å) (Fig. 12). Binding interaction analysis of proposed compounds within HDAC active site demonstrated that Zn^{2+} interacted with oxadiazole N2 (**a** and **d**), oxadiazole N3 and pyrrole NH (**c**). Unexpectedly, although hydroxamate group was previously considered as a Zn^{2+} binding group, but it did not participate in any binding interactions with Zn^{2+} (relatively high distance, 7.02 Å in **a** and 6.41 Å in **b**).

Another interesting point to mention is the lack of ligand-Zn^{2+} interactions in **b** and **e** regarding their similar structural fragments to **a** (Fig. 12). A closer look at intermolecular binding models (Fig. 12) notified that such observation might be attributed to the shortened linker between oxadiazole and pyrrole and also replacement of chiral carbon (**a**) with nitrogen in **b** which induced different inversion pattern. In other words, relatively similar ΔG_b values of **a** and **b** (−9.65 & −9.53 kcal/mol, respectively) might be explained by multiple hydrophobic interactions of **b** via its hydroxamate substituent that could significantly compensate the absence of ligand-Zn^{2+} interactions.

Lack of ligand-Zn^{2+} interactions for **e** may be rationalized by the presence of dichloro dioxane ring despite the presence of identical linker when compared to **a**. Careful inspection of Fig. 12 showed that despite the pyrrole nitrogen, dichloro dioxane of **e** participated in multiple hydrophobic contacts with Leu276 while similar interaction was recorded with just pyrrole ring in **a**. Besides the lack of ligand-Zn^{2+} interactions, lower binding ability of **e** (−8.11 kcal/mol) with regard to **a** and **b**, might be related to fewer H-bond interactions as another important binding feature (Fig. 12e).

3.5. QM studies

N-(3,4-Dichlorobenzyl)-1-[5-(4-bromophenyl)-1,3,4-oxadiazol-2-yl]-1-(1H-pyrrol-2-yl)methanamines (**17**) was previously ranked as one of the most cytotoxic agents in A549 (IC_{50} 17.3 μM) and HT29 (IC_{50} 20 μM) cell lines [25]. In addition; molecular docking simulations recognized **17** as the top-ranked ligand within Bcl-2, EGF, GSK-3 beta, HDAC, telomerase and TS active sites and relatively satisfied *in silico in vitro* correlation model could be established for **17** in the case of telomerase ($R^2 = 0.52$).

In the light of above explanations, **17** might be an appropriate candidate for intermolecular binding energy analysis in terms of individual interacted residues. For this purpose, telomerase complex was introduced into the QM job. Ligand-residue binding energies (ΔE_b) were estimated by Eq. (2):

$$\Delta E_b = E_{LR} - E_R - E_L \quad (2)$$

E_{LR} stands for ligand-residue interaction energy, while E_R and E_L indicate the electronic energies of unbound residues and ligand, respectively. Binding energies of inhibitor (**17**) with individual amino acid residues surrounding the target binding sites at the B3LYP/Def2-SVP level of calculation are summarized in Fig. 13.

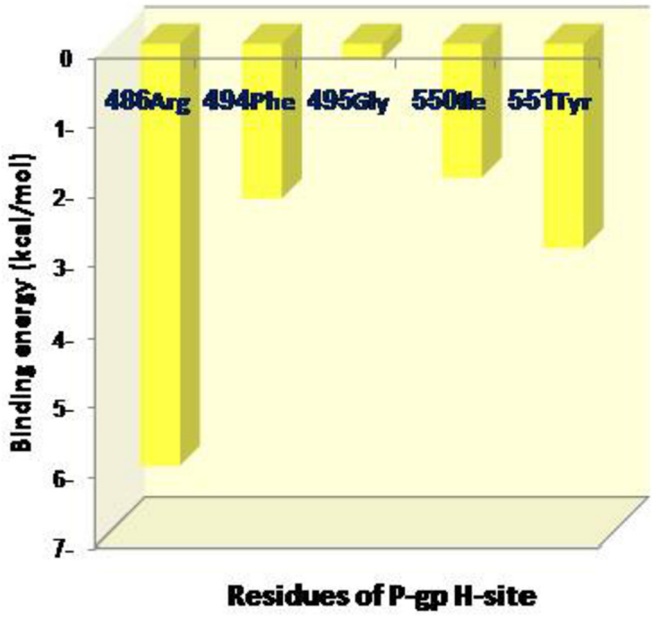

Fig. 13. Ligand-residue binding energies of cancer relevant targets and docked *N*-(3,4-Dichlorobenzyl)-1-[5-(4-bromophenyl)-1,3,4-oxadiazol-2-yl]-1-(1H-pyrrol-2-yl)methanamines (**17**).

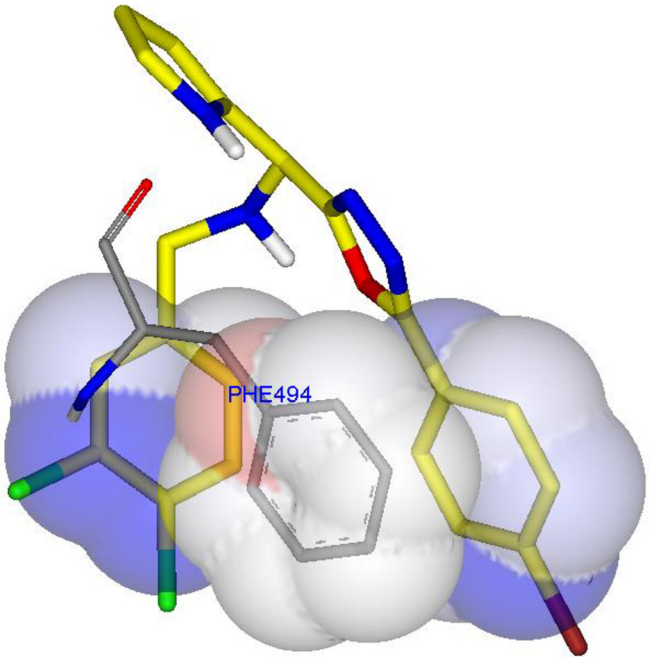

Fig. 14. Possible electrostatic interactions between telomerase active site and compound **17** (PDB ID: **5CQG**), electrostatic surfaces were considered for just phenyl rings of ligand and residue.

As can be understood from the data, lowest binding energy in the B3LYP/Def2-SVP level of calculation was dedicated to Arg486 (−6.05 kcal/mol). 2D schematic representation of interactions indicated that Arg486 might be involved in hydrophobic contact and electrostatic Van der waals interactions with bromophenyl moiety directly attached to the oxadiazole ring. Careful inspection of the 3D interaction diagrams revealed that phenyl ring of Phe494 side chain might be located in an appropriate spatial orientation with regard to both phenyl rings of **17** (Fig. 14). Such stereo orientation might provide a possible π-π stacking contacts within aromatic rings. Moreover it was found that carbonyl oxygen of backbone made H-bond with pyrrole NH (2.69 Å). Ligand-Phe494 interactions were associated with about −2.23 kcal/mol binding energy in our level of study.

Weak binding interactions (binding energy −0.24 kcal/mol) were recorded in the case of Gly495 which participated in hydrophobic contacts within carbon atoms of pyrrole adjacent to NH.

4. Conclusion

Various studies have demonstrated 1,3,4-oxadiazole heterocyclic nucleus as a privileged medicinal scaffold. A series of novel synthesized 2,5-disubstituted 1,3,4-oxadiazole derivatives were subjected to *in silico* analysis of intermolecular binding interactions with some of the cancer relevant oxadiazole-inhibited targets. Structure based computational modeling of novel synthesized cytotoxic (3,4-Dichlorobenzyl)-1-[5-(4-bromophenyl)-1,3,4-oxadiazol-2-yl]-1-(1H-pyrrol-2-yl)methanamines (**1**–**17**) exhibited the contribution of H-bonds, π-π stacking and Van der Waals interactions in potential binding to validated chemotherapeutic targets (ΔG_bs of −5.50 to −12.89 kcal/mol). Molecular docking simulation proposed that candidate oxadiazoles interacted with the active site of MetAP with estimated ΔG_b of −11.20 to −12.92 kcal/mol. In silico structure binding relationship (SBR) studies confirmed that chemical structures possessing chlorine and bromine atoms on 5-substituted phenyl and *N*-benzyl rings (**4** and **17**) exhibited superior binding modes/energies with regard to the majority of studied targets. Binding efficiency as a modern concept for consideration of binding affinity with regard to heavy atom number (efficient binding) was incorporated in our study and it was found that in the case of Bcl-2, EGF, ENR, FAK, GSK-3 beta, telomerase, and VEGF, docked top-ranked ligand also exhibited highest LE values. On the basis of obtained results, a general SAR/SBR pattern for candidate 1,3,4-oxadiazoles were offered and a few hybrid oxadiazole structures were proposed as potential anticancer agents. Intermolecular binding energy analysis was performed on **17** within telomerase as the representative of the best *in silico in vitro* correlated system. On the basis of QM analysis, Arg486, Phe494, Gly495, Ile550, Tyr551 and Arg557 were found to be the dominant attractive residues participating in H-bond and Van der waals interactions within telomerase active site. Since the assessed macromolecular targets were previously proved to be blocked by 1,3,4-oxadiazoles, results of this study might be useful in further design of more potent cytotoxic 1,3,4-oxadiazole derivatives.

Conflicts of interest

Authors declare that they have no conflict of interest.

Acknowledgements

Supports of this project by Research Council of Ardabil University of Medical Sciences are acknowledged.

References

[1] M.R. Yadav, S.T. Shirude, D.S. Putnambekar, P.J. Patel, H.B. Prajapti, A. Parmar, R. Balaraman, R. Giridhar, Studies in 3,4-diaryl-1,2,5-oxadiazoles and their N-oxides: search for better COX-2 inhibitors, Acta Pharm. 57 (2007) 13–30.
[2] Y. Li, J. Liu, H. Zhang, X. Yang, Z. Liu, Stereoselective synthesis and fungicidal activities of (E)-α-(methoxyimino)-benzeneacetate derivatives containing 1,3,4-oxadiazole ring, Bioorg. Med. Chem. Lett 16 (2006) 2278–2282.
[3] W.M. Xu, F.F. Han, M. He, D.Y. Hu, J. He, S. Yang, B.A. Song, Inhibition of tobacco bacterial wilt with sulfone derivatives containing an 1,3,4-oxadiazole moiety, J. Agric. Food Chem. 60 (2012) 1036–1041.
[4] Z. Hajimahdi, A. Zarghi, R. Zabihollahi, M.R. Aghasadeghi, Synthesis, biological evaluation, and molecular modeling studies of new 1,3,4-oxadiazole- and 1,3,4-thiadiazolesubstituted 4-oxo-4H-pyrido[1,2-a] pyrimidines as anti-HIV-1 agents, Med. Chem. Res. 22 (2013) 2467–2475.
[5] S.J. Gilani, S.A. Khan, N. Siddiqui, Synthesis and pharmacological evaluation of condensed heterocyclic 6-substituted 1,2,4-triazolo-[3,4-b]-1,3,4-thiadiazole and 1,3,4-oxadiazole derivatives of isoniazid, Bioorg. Med. Chem. Lett. 20 (2010) 4762–4765.
[6] E. Palaska, G. Sahin, P. Kelicen, N.T. Durlu, G. Altinok, Synthesis and antimicrobial activity of some 1,3,4-oxadiazole derivatives, Farmaco 57 (2002) 539–542.
[7] G.R. Bankar, K. Nandakumar, P.G. Nayak, A. Thakur, M.R. Chamallamudi, G.K. Nampurath, Vasorelaxant effect in rat aortic rings through calcium channel blockage: a preliminary in vitro assessment of a 1,3,4-oxadiazole derivative, Chem. Biol. Interact. 181 (2009) 377–382.
[8] A. Zarghi, S.A. Tabatabai, M. Faizi, A. Ahadian, P. Navabi, V. Zanganeh, A. Shafiee, Synthesis and anticonvulsant activity of new 2-substituted-5-(2-benzyloxyphenyl)-1,3,4-oxadiazoles, Bioorg. Med. Chem. Lett. 15 (2005) 1863–1865.
[9] S. Basu, U.V. Prasad, D.A. Barawkar, S. De, V.P. Palle, S. Menon, M. Patel, S. Thorat, U.P. Singh, K.D. Sarma, Y. Waman, S. Niranjan, V. Pathade, A. Gaur, S. Reddy, S. Ansari, Discovery of novel and potent heterocyclic carboxylic acid derivatives as protein tyrosine phosphatase 1B inhibitors, Bioorg. Med. Chem. Lett. 22 (2012) 2843–2849.
[10] S. Bajaj, V. Asati, J. Singh, P.P. Roy, 1,3,4-Oxadiazoles: an emerging scaffold to target growth factors, enzymes and kinases as anticancer agents, Eur. J. Med. Chem. 97 (2015) 124–141.
[11] Q.Z. Zheng, X.M. Zhang, Y. Xu, K. Cheng, Q.C. Jiao, H.L. Zhu, Synthesis, biological evaluation, and molecular docking studies of 2-chloropyridine derivatives possessing 1,3,4-oxadiazole moiety as potential antitumour agents, Bioorg. Med. Chem. 18 (2010) 7836–7841.
[12] X.M. Zhang, M. Qiu, J. Sun, Y.B. Zhang, Y.S. Yang, X.L. Wang, H.L. Zhu, Synthesis, biological evaluation, and molecular docking studies of 1,3,4-oxadiazole derivatives possessing 1,4-benzodioxan moiety as potential anticancer agents, Bioorg. Med. Chem. 19 (2011) 6518–6524.
[13] J. Sun, H. Zhu, Z.M. Yang, H.L. Zhu, Synthesis, molecular modeling and

biological evaluation of 2 aminomethyl-5-(quinolin-2-yl)-1,3,4-oxadiazole-2(3H)-thione quinolone derivatives as novel anticancer agent, Eur. J. Med. Chem. 60 (2013) 23–28.
[14] F. Zhang, X.L. Wang, J. Shi, S.F. Wang, Y. Yin, Y.S. Yang, W.M. Zhang, H.L. Zhu, Synthesis, molecular modeling and biological evaluation of *N*-benzylidene-2-((5-(pyridin-4-yl)-1,3,4-oxadiazol-2-yl) thio) acetohydrazide derivatives as potential anticancer agents, Bioorg. Med. Chem. 22 (2014) 468–477.
[15] H. Rajak, A. Agarawal, P. Parmar, B.S. Thakur, R. Veerasamy, P.C. Sharma, M.D. Kharya, 2,5-Di-substituted-1,3,4-oxadiazoles/thiadiazole as surface recognition moiety: design and synthesis of novel hydroxamic acid based Histone deacetylase inhibitors, Bioorg. Med. Chem. Lett. 21 (2011) 5735–5738.
[16] M. Suenaga, H. Soda, M. Oka, A. Yamaguchi, K. Nakatomi, K. Shiozawa, S. Kawabata, T. Kasai, Y. Yamada, S. Kamihira, C. Tei, S. Kohno, Histone deacetylase inhibitors suppress telomerase reverse transcriptase mRNA expression in prostate cancer cells, Int. J. Canc. 97 (5) (2002) 621–625.
[17] M. Medina, A. Castro, Glycogen synthase kinase-3 (GSK-3) inhibitors reach the clinic, Curr. Opin. Drug. Discov. Dev. 11 (4) (2008) 533–543.
[18] J. Sun, M.H. Li, S.S. Qian, F.J. Guo, X.F. Dang, X.M. Wang, Y.R. Xue, H.L. Zhu, Synthesis and antitumour activity of 1,3,4-oxadiazole possessing 1,4-benzodioxan moiety as a novel class of potent methionine aminopeptidase type II inhibitors, Bioorg. Med. Chem. Lett. 23 (2013) 2876–2879.
[19] S. Zhang, Y. Luo, L.Q. He, Z.J. Liu, H.L. Zhu, Synthesis, biological evaluation, and molecular docking studies of novel 1,3,4-oxadiazole derivatives possessing benzotriazole moiety as FAK inhibitors with anticancer activity, Bioorg. Med. Chem. 21 (2013) 3723–3729.
[20] L.R. Zhang, Z.J. Liu, H. Zhang, J. Sun, Y. Luo, T.T. Zhao, H.B. Gong, H.L. Zhu, Synthesis, biological evaluation and molecular docking studies of novel 2-(1,3,4-oxadiazol-2-ylthio)-1-phenylethanone derivatives, Bioorg. Med. Chem. 20 (2012) 3615–3621.
[21] Q.R. Du, D.D. Li, Y.Z. Pi, J.R. Li, J. Sun, F. Fang, W.Q. Zhong, H.B. Gong, H.L. Zhu, Novel 1,3,4-oxadiazole thioether derivatives targeting thymidylate synthase as dual anticancer/antimicrobial agents, Bioorg. Med. Chem. 21 (2013) 2286–2297.
[22] Z.W. Cai, D. Wei, R.M. Borzilleri, L. Qian, A. Kamath, S. Mortillo, B. Wautlet, B.J. Henley, R. Jeyaseelan, S.J. Tokarski, J.T. Hunt, R.S. Bhide, J. Fargnoli, L.J. Lombardo, Synthesis, SAR, and evaluation of 4 [2,4Difluoro-5 (cyclopropylcarbamoyl) phenylamino]pyrrolo [2,1-f] [1,2,4]triazine-based VEGFR-2 kinase inhibitors, Bioorg. Med. Chem. Lett. 18 (2008) 1354–1358.
[23] R. Ruel, C. Thibeault, A. L'Heureux, A. Martel, Z.W. Cai, D. Wei, L. Qian, J.C. Barrish, A. Mathur, C. D'Arienzo, J.T. Hunt, A. Kamath, P. Marathe, Y. Zhang, G. Derbin, B. Wautlet, S. Mortillo Sr., S. Jeyaseelan, B. Henley, R. Tejwani, R.S. Bhide, G.L. Trainor, J. Fargnolib, L.J. Lombardo, Discovery and preclinical studies of 5-isopropyl-6-(5-methyl-1,3,4-oxadiazol-2-yl)-N-(2-methyl-1H-pyrrolo[2,3-b]pyridin-5-yl)pyrrolo[2,1-f][1,2,4]triazin-4-amine (BMS-645737), an in vivo active potent VEGFR-2 inhibitor, Bioorg. Med. Chem. Lett 18 (2008) 2985–2989.
[24] S.M.A. Seri, Synthesis and biological evaluation of novel 2,4-bis substituted diphenylamines as anticancer agents and potential epidermal growth factor receptor tyrosine kinase inhibitors, Eur. J. Med. Chem. 45 (2010) 4113–4121.
[25] A. Ramazani, M. Khoobi, A. Torkaman, F. Zeinali Nasrabadi, H. Forootanfar, M. Shakibaei, M. Jafari, A. Ameri, S. Emami, M.A. Faramarzi, A. Foroumandi, A. Shafiee, One-pot, four-component synthesis of novel cytotoxic agents 1-(5-aryl-1,3,4-oxadiazol-2 -yl)-1-(1 H-pyrrol-2-yl)methanamines, Eur. J. Med. Chem. 78 (2014) 151–156.
[26] C.A. Lipinski, Drug-like properties and the causes of poor solubility and poor permeability, J. Pharmacol. Toxicol. Meth. 44 (1) (2000) 235–249.
[27] H.L. Perez, P. Banfi, J.A. Bertrand, Z.W. Cai, J.W. Grebinski, K. Kim, J. Lippy, M. Modugno, J. Naglich, R.J. Schmidt, A. Tebben, P. Vianello, D.D. Wei, L. Zhang, A. Galvani, L.J. Lombardo, R.M. Borzilleri, Identification of a phenylacylsulfonamide series of dual Bcl-2/Bcl-Xl antagonists, Bioorg. Med. Chem. Lett. 22 (2012) 3946–3950.
[28] Y. Kawakita, M. Seto, T. Ohashi, T. Tamura, T. Yusa, H. Miki, H. Iwata, H. Kamiguchi, T. Tanaka, S. Sogabe, Y. Ohta, T. Ishikawa, Design and synthesis of novel pyrimido[4,5-b]azepine derivatives as HER2/EGFR dual inhibitors, Bioorg. Med. Chem. 21 (2013) 2250–2261.
[29] M.J. Stewart, S. Parikh, G. Xiao, P.J. Tonge, C. Kisker, Structural basis and mechanism of enoyl reductase inhibition by triclosan, J. Mol. Biol. 290 (1999) 859–865.
[30] U. Gradler, J. Bomke, D. Musil, V. Dresing, M. Lehmann, G. Holzemann, H. Greiner, C. Esdar, M. Krier, T. Heinrich, Fragment-based discovery of focal adhesion kinase inhibitors, Bioorg. Med. Chem. Lett. 23 (2013) 5401–5409.
[31] J.A. Bertrand, S. Thieffine, A. Vulpetti, C. Cristiani, B. Valsasina, S. Knapp, H.M. Kalisz, M. Flocco, Structural characterization of the Gsk-3Beta active site using selective and non-selective ATP-mimetic inhibitors, J. Mol. Biol. 333 (2003) 393–407.
[32] F.F. Wagner, M. Weiwer, S. Steinbacher, A. Schomburg, P. Reinemer, J.P. Gale, A.J. Campbell, S.L. Fisher, W.N. Zhao, S.A. Reis, K.M. Hennig, M. Thomas, P. Muller, M.R. Jefson, D.M. Fass, S.J. Haggarty, Y.L. Zhang, E.B. Holson, Kinetic and structural insights into the binding of histone deacetylase 1 and 2 (HDAC1, 2) inhibitors, Bioorg. Med. Chem. 24 (2016) 4008–4015.
[33] G.S. Sheppard, J. Wang, M. Kawai, S.D. Fidanze, N.Y. BaMaung, S.A. Erickson, D.M. Barnes, J.S. Tedrow, L. Kolaczkowski, A. Vasudevan, D.C. Park, G.T. Wang, W.J. Sanders, R.A. Mantei, F. Palazzo, L. Tucker-Garcia, P. Lou, Q. Zhang, C.H. Park, K.H. Kim, A. Petros, E. Olejniczak, D. Nettesheim, P. Hajduk, J. Henkin, R. Lesniewski, S.K. Davidsen, R.L. Bell, Discovery and optimization of anthranilic acid sulfonamides as inhibitors of methionine aminopeptidase-2: a structural basis for the reduction of albumin binding, J. Med. Chem. 49 (2006) 3832–3849.
[34] C. Bryan, C. Rice, H. Hoffman, M. Harkisheimer, M. Sweeney, E. Skordalakes, Structural basis of Telomerase inhibition by the highly specific BIBR1532, Structure 23 (10) (2015) 1934–1942.
[35] A. Dowiercial, A. Jarmula, P. Wilk, W. Rypniewski, M. Kowalska, T. Fraczyk, J. Ciesla, W. Rode, Mouse thymidylate synthase does not show the inactive conformation, observed for the human enzyme, Struct. Chem. 28 (3) (2017) 667–674.
[36] N. Miyamoto, N. Sakai, T. Hirayama, K. Miwa, Y. Oguro, H. Oki, K. Okada, T. Takagi, H. Iwata, Y. Awazu, S. Yamasaki, T. Takeuchi, H. Miki, A. Hori, S. Imamura, Discovery of *N*-[5-({2 [(cyclopropylcarbonyl)amino]imidazo[1,2-b]pyridazin-6-yl}oxy)-2-methylphenyl]-1,3-dimethyl-1H-pyrazole-5-carboxamide (TAK-593), a highly potent VEGFR2 kinase inhibitor, Bioorg. Med. Chem. 21 (2013) 2333–2345.
[37] G.M. Morris, R. Huey, A.J. Olson, Using AutoDock for ligand-receptor docking, Curr. Protoc. Bioinfo. 11 (2008) 34–37.
[38] N. Razzaghi-Asl, A. Ebadi, N. Edraki, A. Mehdipour, S. Shahabipour, R. Miri, Response surface methodology in docking study of small molecule BACE-1 inhibitors, J. Mol. Model. 18 (2012) 4567–4576.
[39] P.E. Czabotar, G. Lessene, A. Strasser, J.M. Adams, Control of apoptosis by the BCL-2 protein family: implications for physiology and therapy, Nat. Rev. Mol. Cell Biol. 15 (2014) 49–63.
[40] M.K. Mohammadi, O. Firuzi, M. Khoshneviszadeh, N. Razzaghi-Asl, S. Sepehri, R. Miri, Novel 9-(alkylthio)-Acenaphtho[1,2-e]-1,2,4-triazine derivatives: synthesis, cytotoxic activity and molecular docking studies on B-cell lymphoma 2 (Bcl-2). DARU, J. Pharm. Sci. 22 (2014) 2.
[41] Y. Tsujimoto, L.R. Finger, J. Yunis, P.C. Nowell, C.M. Croce, Cloning of the chromosome breakpoint of neoplastic B cells with the t (14; 18) chromosome translocation, Science 226 (1984) 1097–1099.
[42] R. Bianco, T. Gelardi, V. Damiano, F. Ciardiello, G. Tortora, Rational bases for the development of EGFR inhibitors for cancer treatment, Int. J. Biochem. Cell Biol. 39 (2007) 1416–1431.
[43] T. Sasada, K. Azuma, J. Ohtake, Y. Fujimoto, Immune responses to epidermal growth factor receptor (EGFR) and their application for cancer treatment, Front. Pharmacol. 7 (2016) 405.
[44] K.H. Sippel, N.K. Vyas, W. Zhang, B. Sankaran, F.A. Quiocho, Crystal structure of the human fatty acid synthase enoyl-acyl Carrier protein-reductase domain complexed with triclosan reveals allosteric protein protein interface inhibition, J. Biol. Chem. 289 (48) (2014) 33287–33295.
[45] P.L. Alo, P. Visca, A. Marci, A. Mangoni, C. Botti, U. Di Tondo, Expression of fatty acid synthase (FAS) as a predictor of recurrence in stage I breast carcinoma patients, J. Canc. 77 (1996) 474–482.
[46] F.J. Sulzmaier, C. Jean, D.D. Schlaepfer, FAK in cancer: mechanistic findings and clinical applications, Nat. Rev. Canc. 14 (2014) 598–610.
[47] Y.T. Huang, L. Zhao, Z. Fu, M. Zhao, X.M. Song, J. Jia, S. Wang, J.P. Li, Z.F. Zhu, G. Lin, R. Lu, Z. Yao, Therapeutic effects of tyroservatide on metastasis of lung cancer and its mechanism affecting integrin-focal adhesion kinase signal transduction, Drug Des. Dev. Ther. 10 (2016) 649–663.
[48] A. Alowayed, M.S. Salker, N. Zeng, Y. Singh, F. Lang, LEFTY2 controls migration of human endometrial cancer cells *via* focal adhesion kinase activity (FAK) and miRNA-200a, Cell. Physiol. Biochem. 39 (2016) 815–826.
[49] J.A. McCubrey, T.L. Fitzgerald, L.V. Yang, K. Lertpiriyapong, L.S. Steelman, S.L. Abrams, G. Montalto, M. Cervello, L.M. Neri, L. Cocco, A.M. Martelli, P. Laidler, J. Dulińska-Litewka, D. Rakus, A. Gizak, F. Nicoletti, L. Falzone, S. Candido, M. Libra, Roles of GSK-3 and microRNAs on epithelial mesenchymal transition and cancer stem cells, Oncotarget 8 (8) (2017) 14221–14250.
[50] J.A. McCubrey, L.S. Steelman, F.E. Bertrand, N.M. Davis, M. Sokolosky, S.L. Abrams, G. Montalto, A.B. D'Assoro, M. Libra, F. Nicoletti, R. Maestro, J. Basecke, D. Rakus, A. Gizak, Z.N. Demidenko, L. Cocco, A.M. Martelli, M. Cervello, GSK-3 as potential target for therapeutic intervention in cancer, Oncotarget 5 (10) (2014) 2881–2911.
[51] M. Nakagawa, Y. Oda, T. Eguchi, S. Aishima, T. Yao, F. Hosoi, Y. Basaki, M. Ono, M. Kuwano, M. Tanaka, M. Tsuneyoshi, Expression profile of class I histone deacetylases in human cancer tissues, Oncol. Rep. 18 (2007) 769–774.
[52] A.A. Lane, B.A. Chabner, Histone deacetylase inhibitors in cancer therapy, J. Clin. Oncol. 27 (32) (2009) 5459–5468.
[53] S. Ropero, M. Esteller, The role of histone deacetylases (HDACs) in human cancer, J. Mol. Oncol. 1 (2007) 19–25.
[54] S.Y. Chang, E.C. McGary, S. Chang, Methionine aminopeptidase gene of Escherichia coli is essential for cell growth, J. Bacteriol. 171 (1989) 4071–4072.
[55] R.G. Krishna, F. Wold, Post-translational modification of proteins, Adv. Enzymol. Relat. Area Mol. Biol. 67 (1993) 265–298.
[56] P. Selvakumar, A. Lakshmikuttyamma, J.R. Dimmock, R.K. Sharma, Methionine aminopeptidase 2 and cancer, Biochim. Biophys. Acta 1765 (2006) 148–154.
[57] J.M. Martínez, I. Prieto, M.J. Ramírez, C. Cueva, F. Alba, M. Ramírez, Aminopeptidase activities in breast cancer tissue, Clin. Chem. 45 (1999) 1797–1802.
[58] P. Selvakumar, A. Lakshmikuttyamma, R. Kanthan, S.C. Kanthan, J.R. Dimmock, R.K. Sharma, High expression of methionine aminopeptidase 2 in human colorectal adenocarcinomas, Clin. Canc. Res. 10 (2004) 2771–2775.
[59] K. Masutomi, E.Y. Yu, S. Khurts, I. Ben-Porath, J.L. Currier, G.B. Metz,

M.W. Brooks, S. Kaneko, S. Murakami, J.A. DeCaprio, R.A. Weinberg, S.A. Stewart, W.C. Hahn, Telomerase maintains telomere structure in normal human cells, Cell 114 (2003) 241–253.
[60] M. Ivancich, Z. Schrank, L. Wojdyla, B. Leviskas, A. Kuckovic, A. Sanjali, N. Puri, Treating cancer by targeting telomeres and telomerase, Antioxidants 6 (1) (2017) 15.
[61] A.P. Cunninghama, W.K. Lovea, R.W. Zhang, L.G. Andrewsa, T.O. Tollefsbol, Telomerase inhibition in cancer therapeutics: molecular-based approaches, J. Curr. Med. Chem. 13 (24) (2006) 2875–2888.
[62] M. Choi, K. Karunaratne, A. Kohen, Flavin-dependent thymidylate synthase as a new antibiotic target, Molecules 21 (5) (2016) 654.
[63] X. Lin, L.A. Parsels, D.M. Voeller, C.J. Allegra, G.F. Maley, F. Maley, E. Chu, Characterization of a *cis*-acting regulatory element in the protein coding region of thymidylate synthase mRNA, Nucleic Acids Res. 28 (2000) 1381–1389.
[64] Y. Zhao, A.A. Adjei, Targeting angiogenesis in cancer therapy: moving beyond vascular endothelial growth factor, Oncol. 20 (2015) 660–673.
[65] D.J. Hicklin, L.M. Ellis, Role of the vascular endothelial growth factor pathway in tumor growth and angiogenesis, J. Clin. Oncol. 23 (2005) 1011–1027.
[66] E. Roberts, D.A.F. Cossigny, G.M.Y. Guan, The role of vascular endothelial growth factor in metastatic prostate cancer to the skeleton, Prostate Canc. (2013), 418340.
[67] G.M. Morris, R. Huey, W. Lindstrom, M.F. Sanner, R.K. Belew, D.S. Goodsell, A.J. Olson, AutoDock4 and AutoDockTools4: automated docking with selective receptor flexibility, J. Comput. Chem. 30 (2009) 2785–2791.
[68] G.M. Morris, D.S. Goodsell, R.S. Halliday, R. Huey, W.E. Hart, R.K. Belew, A.J. Olson, Automated docking using a Lamarckian genetic algorithm and an empirical binding free energy function, J. Comput. Chem. 19 (1998) 1639–1662.
[69] A.C. Wallace, R.A. Laskowski, J.M. Thornton, LIGPLOT: a program to generate schematic diagrams of protein-ligand interactions, Protein Eng. 8 (1995) 127–134.
[70] G. Fogarasi, X. Zhou, P.W. Taylor, P. Pulay, The calculation of ab initio molecular geometries: efficient optimization by natural internal coordinates and empirical correction by off wet forces, J. Am. Chem. Soc. 114 (1992) 8191–8201.
[71] F. Neese, ORCA - an Ab Initio, Density Functional and Semiempirical Program Package. Version 2.8.0, Edn, University of Bonn, 2011.
[72] S. Putta, P. Beroza, Shapes of things: computer modeling of molecular shape in drug discovery, Curr. Top. Med. Chem. 7 (15) (2007) 1514–1524.
[73] R. Laurie, T. Alasdair, R.M. Jackson, Methods for the prediction of protein-ligand binding sites for structure-based drug design and virtual ligand screening, Curr. Protein Pept. Sci. 7 (5) (2006) 395–406.
[74] R.P. Sellers, L.D. Alexander, V.A. Johnson, C.C. Lin, J. Savage, R. Corral, J. Moss, T.S. Slugocki, E.K. Singh, M.R. Davis, Design and synthesis of Hsp90 inhibitors: exploring the SAR of Sansalvamide A derivatives, Bioorg. Med. Chem. Lett. 18 (18) (2010) 6822–6856.
[75] N. Razzaghi-Asl, O. Firuzi, B. Hemmateenejad, K. Javidnia, N. Edraki, R. Miri, Design and synthesis of novel 3,5-bis-*N*-(aryl/heteroaryl) carbamoyl-4-aryl-1,4-dihydropyridines as small molecule BACE-1 inhibitors, Bioorg. Med. Chem. 21 (22) (2013) 6893–6909.
[76] A.L. Hopkins, C.R. Groom, A. Alex, Ligand efficiency: a useful metric for lead selection, Drug Discov. Today 9 (10) (2004) 430–431.
[77] H. Rajak, A. Agarawal, P. Parmar, B.S. Thakur, R. Veerasamy, P.C. Sharma, M.D. Kharya, 2,5-Di-substituted-1,3,4-oxadiazoles/thiadiazole as surface recognition moiety: design and synthesis of novel hydroxamic acid based histone deacetylase inhibitors, Bioorg. Med. Chem. Lett. 21 (2011) 5735–5738.